Innovation of Chemistry & Materials for Sustainability
Volume 2, Issue 2, July- Dec. **2025**
RESEARCH ARTICLE
ISSN (Print): 3049 – 2548
ISSN (Online): 3049 – 0146

Effect of Zirconia Crystalline Phases on Pt Dispersion and Catalytic Performance in Alkyne Hydrosilylation

Yuki Aoki[a], Anas Abdullahi[a], Mustapha G. Mohammed[b], Kotaro Kawaguchi[a], and Kazu Okumura[a]*

[a]Department of Applied Chemistry, School of Advanced Engineering, Kogakuin University, 2665-1 Nakano-machi Hachioji-city, 192-0015, Tokyo, Japan.
[b]Department of Chemical Engineering, Faculty of Engineering, Universiti Malaya, 50603, Kuala Lumpur, Malaysia.

*Correspondence: okmr@cc.kogakuin.ac.jp (K. Okumura)

Abstract: The crystalline phase of catalyst support plays a crucial role in governing the dispersion and activity of supported metal species. Herein, we investigate the influence of amorphous (a-), monoclinic (m-), and tetragonal ZrO_2 (t-ZrO_2) support on the performance of Pt/ZrO_2 catalysts in the hydrosilylation of alkynes. Catalysts supported on m-ZrO_2 and t-ZrO_2 exhibited high Pt dispersion and catalytic activity, while those supported on a-ZrO_2 showed poor performance due to encapsulation of Pt during heat treatment. When a-ZrO_2 was calcined, it underwent a transformation to the monoclinic phase, which improved the dispersion and catalytic activity of the supported Pt. Structural and spectroscopic analyses including XRD, H_2-TPR, Pt L_3-edge EXAFS, and CO chemisorption revealed that the monoclinic and tetragonal phase uniquely stabilizes Pt at or near the surface. However, when comparing Pt/m-ZrO_2 and Pt/t-ZrO_2, the former showed higher dispersion and better reusability than the latter. These findings highlight the critical role of ZrO_2 support crystallinity in tuning metal-support interactions and establish m-ZrO_2 as promising platform for designing efficient hydrosilylation catalysts.

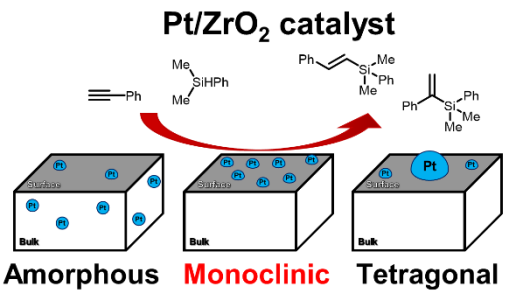

Keywords: *Hydrosilylation, Alkyne, Pt Catalysts, Monoclinic Zirconia, Metal Dispersion*

1. Introduction

Hydrosilylation is a fundamental catalytic reaction involving the addition of hydrosilanes to unsaturated organic compounds.[1] It is extensively employed in the synthesis of organosilicon materials, silicones, and fine chemicals,[2] owing to its high atom efficiency and ability to produce valuable silicon-containing products with precise functionalization.[3] Hydrosilane has been also used to generate Ni-H species in cross-coupling reactions on nickel catalysts.[4] Platinum (Pt) is the benchmark metal catalyst for the hydrosilylation, due to its outstanding activity, selectivity and ability to provide high turnover numbers (TONs).[4-11] Industrial processes predominantly utilize homogeneous Pt catalysts, particularly the Speier catalyst (H_2PtCl_6) and the Karstedt catalyst ($O[Si(CH_3)_2CH=CH_2]_2Pt$). However, their homogeneous nature presents drawbacks, including catalyst separation issues, metal leaching, and limited recyclability. Notably, approximately 5.6 tons of Pt were irretrievably lost in hydrosilylation processes in 2007 alone.[12] To mitigate these limitations, heterogeneous Pt catalysts have been explored, yet they often exhibit reduced efficiency due to incomplete exposure of active sites, resulting in lower TON. Recent efforts have focused on achieving near-single-atom dispersion to match the performance of homogeneous systems, highlighting the direct correlation between catalytic activity and metal dispersion.[13] For example, single-site Pt catalysts supported on Al_2O_3 or TiO_2 exhibit remarkable activity in hydrosilylations.[14] Pt/-Al_2O_3-IP, prepared by impregnating $H_2PtCl_6{\cdot}H_2O$ into alumina nanorods, achieved six reuse cycles and a maximum turnover number (TON) of 3×10^5.[15] Similarly, the single-site Pt on TiO_2 ($Pt^{\delta+}/TiO_2$) was reported to be active and recycle in the reaction. Density functional theory calculations revealed that its high activity stems from the atomic dispersion of active species and the partially positively charged $Pt^{\delta+}$ electronic structure.[16] In another study, Pt was loaded on graphene with microwave irradiation as a precursor for $PtCl_4^{2-}$. The resulting catalyst exhibited a turnover frequency (TOF) of 4.8×10^6 h^{-1} and a TON of 9.4×10^6, enabling continuous hydrosilylation in a packed-bed reactor.[17] Our laboratory previously demonstrated that highly dispersed Ru on ZrO_2 calcined at 800 °C, exhibited excellent activity in benzyl alcohol oxidation, suggesting that appropriate thermal treatment can enhance metal dispersion on ZrO_2 supports.[18] Additionally, metal-support interaction[19] and electrostatic effects[20] have been identified as key factors promoting Pt/ZrO_2 catalyzed hydrosilylation. We have recently reported that Pt catalysts supported on ZrO_2 and CeO_2 exhibit high activity and recyclability in the hydrosilylation reactions of alkenes and alkynes.[21] Furthermore, in our research on Ru/ZrO_2 catalysts prepared by the solid-phase method, we clarified that when m-ZrO_2 is used as a support, atomic Ru is generated and exhibits high catalytic activity in various reactions including benzyl alcohol oxidation, levulinic acid hydrodeoxygenation, and ammonia decomposition, but when t-ZrO_2 is used as the support, Ru is not dispersed and exhibits negligible activity. We also found that adjusting the calcination temperature of m-ZrO_2 to about 800 °C is also important for Ru to develop high catalytic activity.[18] These findings mean that the crystalline phase of ZrO_2 has a significant effect on the dispersion, structure, and catalytic activity of Ru.[22] Therefore,

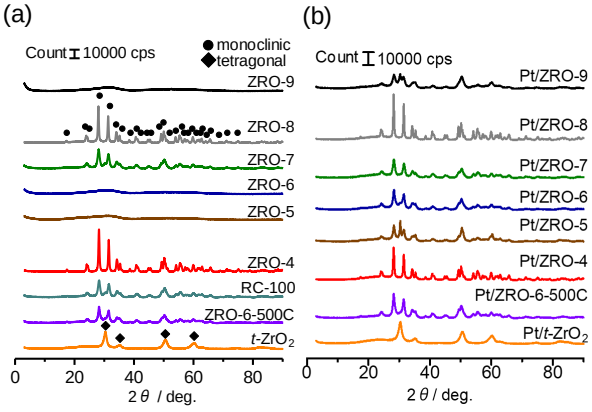

Figure 1. *(a) XRD patterns of the unloaded ZrO_2 supports (b) Pt-loaded ZrO_2 catalysts calcined at 500 °C (Pt loading: 0.7 wt%).*

https://doi.org/10.63654/icms.2025.02171
Innov. Chem. Mater. Sustain. **2025**, *2*(2), 171-176
Received: 26 August 2025; Revised: 26 October 2025; Accepted: 02 November 2025; Published (online): 15 November 2025

we were interested in how the crystalline phase of the ZrO_2 support affects the degree of Pt dispersion and catalytic activity. In this study, we investigated the structure-activity relationship of Pt supported on ZrO_2 by systematically comparing catalysts prepared on amorphous, monoclinic and tetragonal phases. We focused on how support crystal phase and thermal treatment temperature influenced on Pt dispersion and, consequently, hydrosilylation performance of Pt for an alkyne molecule. Since Pt catalysts are used not only for hydrosilylation reactions but also for many other catalytic reactions, it is very important to establish a method for the preparation of Pt catalysts with high dispersibility.

2. Results and Discussion

Reactions using alkyne as a substrate

To study the effect of support and thermal treatment Figure 1a and 1b present the XRD patterns of the unloaded ZrO_2 supports and Pt-loaded ZrO_2 catalysts (Pt loading: 0.7 wt%) calcined at 500 °C, respectively. The t-ZrO_2 (t-ZrO_2) phase is noted where applicable. The as-received ZRO-4, ZRO-7, ZRO-8 and RC-100 exhibited diffraction peaks characteristic of m-ZrO_2, whereas JRC-ZRO-5, JRC-ZRO-6, and JRC-ZRO-9 displayed broad, featureless patterns, indicative of an amorphous phase. Upon loading of Pt, followed by calcination at 500 °C (Figure 1b), the initially amorphous supports ZRO-5, ZRO-6, and ZRO-9 underwent phase transformation into monoclinic as well as tetragonal phases, as evidenced by the emergence of distinct peaks corresponding to m-ZrO_2 and t-ZrO_2. The specific surface area of the catalysts, shown in Figure S1, reveals an inverse relationship between crystallinity and specific surface area. Specifically, Pt/ZRO-4 and Pt/ZRO-8, which exhibited higher XRD diffraction intensities, correspondingly displayed lower surface areas. This trend suggests that increased crystallite size in these ZrO_2 supports reduces the available surface area, consistent with their higher degree of crystallinity. The Pt L_3-edge EXAFS of these samples appeared only Pt-O bonds, indicating that Pt was well dispersed on the ZrO_2 surface (Figure S2). Indeed, diffraction arising from metallic Pt, which typically appears around 39.8° (Pt(111)), was not observed in the enlarged XRD pattern (Figure S3). Measurements of X-ray photoelectron spectroscopy (XPS) of Pt/m-ZrO_2 calcined at 500 °C revealed a spectral position (photon energy) was close to that of PtO_2, suggesting the valence of Pt on m-ZrO_2 was predominantly +4 (Figure S4).

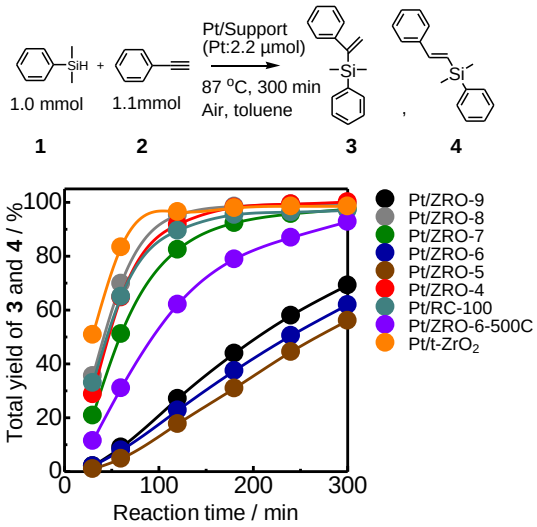

Figure 2. *Time-dependent variation in the yield of products* **3**, **4**.

Figure 2 presents the time-dependent product yields (products **3** and **4**) for the hydrosilylation of ethynylbenzene

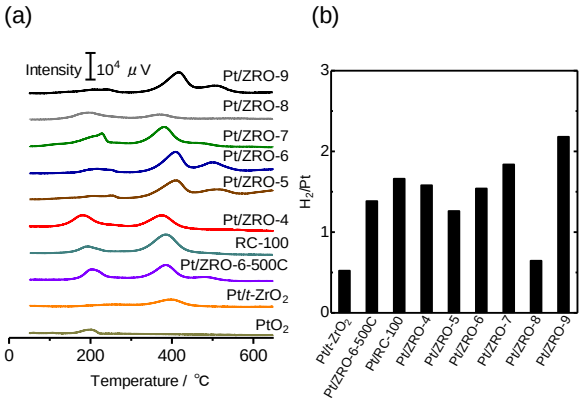

Figure 3. *(a) H_2-TPR profiles of the PtO_2 and Pt/ZrO_2. (b) H_2/Pt molar ratios calculated from the hydrogen consumption peak areas in H_2-TPR.*

over the prepared catalysts. The products of the hydrosilylation reaction (mixture of **3** and **4**) were measured by ^{1}H and ^{13}C NMR (Figure S5), and their spectra were confirmed to match those reported in the literature.[23] As confirmed by the gas chromatograph (GC) chart show in Figure S6, the ratio of products **3** and **4** was approximately 1:2. Among the catalysts, Pt/t-ZrO_2, Pt/ZRO-4, Pt/ZRO-7, Pt/ZRO-8, and Pt/RC-100 exhibited relatively higher activity. In contrast, Pt/ZRO-5, Pt/ZRO-6, and Pt/ZRO-9 showed markedly lower product yields. This trend reveals a strong correlation between the crystalline phase of the ZrO_2 support and catalytic performance; Pt catalysts supported on t-ZrO_2, and m-ZrO_2 (Pt/ZRO-4, -7, and -8) were highly active, while those supported on a-ZrO_2 (Pt/ZRO-5, -6, and -9) were the least active. These observations suggest that the crystallographic phase of the ZrO_2 support critically influences the dispersion and catalytic performance of Pt in the hydrosilylation reaction. Notably, Pt/ZRO-4 (30 m^2g^{-1}) and Pt/ZRO-8 (24 m^2g^{-1}) achieved high catalytic performance despite their relatively low specific surface areas. This shows that under current conditions, surface area does not determine the activity of Pt. However, the possible contributions of extremely low surface area or variations in Pt dispersion and loading cannot be entirely excluded and warrant further investigation.

Figure 3(a) displays the H_2-TPR profiles of the Pt/ZrO_2 catalysts. A prominent reduction peak approximately at 200 °C, attributed to the reduction of PtO_2, was observed across all samples and consistent with the profile of pure PtO_2. Notably, the Pt/t-ZrO_2 sample exhibited only a trace of this peak, implying that the Pt species were highly dispersed, likely close to atomic dispersion, resulting in minimal hydrogen consumption. The minor peak at 400 °C may indicate that Pt strongly interact with ZrO_2. In contrast, Pt/ZRO-4 and Pt/ZRO-7 both supported on m-ZrO_2, showed much more intense peaks at 200 °C, indicative of a greater abundance of reducible Pt species. Although Pt/ZRO-8 also demonstrated high catalytic activity, its overall H_2 uptake was lower; however, the intensity ratio between the 200 °C and 400 °C peaks remained consistent with that of the other monoclinic-supported catalysts. These observations suggest a phase-dependent interaction between Pt and the support, with m-ZrO_2 favoring the formation of readily reducible Pt species. A second reduction peak around 400 °C, absent in pure PtO_2, was observed for all ZrO_2-supported catalysts regardless of phase, and is attributed to hydrogen consumption associated with the ZrO_2 support itself or Pt species that strongly interacted with ZrO_2. The invariance of this peak across tetragonal, monoclinic, and amorphous phases suggests that it is structurally agnostic. A third, higher-temperature peak at ~500 °C appeared exclusively in catalysts supported on a-ZrO_2 (Pt/ZRO-5, Pt/ZRO-6, and Pt/ZRO-9). This is indicative of a stronger metal-support interactions, where PtO_2 may be more stable oxidation state, requiring higher temperatures for

reduction. This stronger interaction may contribute to the lower catalytic activity observed for these samples, due to a reduced number of active, accessible Pt species. Figure 3(b) presents the H_2/Pt molar ratios calculated from the hydrogen consumption peak areas in the H_2-TPR profiles. These ratios provide a semi-quantitative measure of Pt dispersion and accessibility. Pt/t-ZrO_2 and Pt/ZRO-8 exhibited notably lower H_2/Pt ratios compared to the other catalysts. This trend likely reflects a higher degree of Pt^0 dispersion on these supports. In such cases, the reduced coordination environment of Pt atoms can lead to lower hydrogen uptake per Pt atom, as fewer hydrogen molecules are required for reduction. These findings corroborate the enhanced catalytic activity observed for Pt/t-ZrO_2 and Pt/ZRO-8 underscoring the role of high metal dispersion in facilitating efficient hydrosilylation.

Figure 4 presents the relationship between Pt dispersion, determined by CO pulse chemisorption, and the total yield of products **3** and **4** after 60 minutes of the hydrosilylation reaction. A strong positive correlation was observed between Pt dispersion and catalytic performance. Pt/t-ZrO_2, which exhibited the highest dispersion, also achieved the greatest yield, followed by Pt/ZRO-4, Pt/ZRO-7, Pt/ZRO-8, and Pt/RC-100 all of which are supported on m-ZrO_2 and showed relatively high Pt dispersion. In contrast, Pt/ZRO-5, Pt/ZRO-6, and Pt/ZRO-9, supported on a-ZrO_2, exhibited significantly lower dispersions and correspondingly reduced catalytic activity. These results underscore the critical role of metal dispersion in determining hydrosilylation efficiency, where a higher number of surface-exposed Pt sites enhances catalytic performance. The reduced dispersion of Pt on a-ZrO_2 supports is likely due to the encapsulation of Pt into ZrO_2 during heat treatment, which coincides with the amorphous-to-monoclinic or to tetragonal phase transformation. During this crystallization process, Pt species may become encapsulated within the growing ZrO_2 crystallites due to increased proximity of Pt species, leading to a decrease in Pt atoms being exposed on the surface. The fact that Pt is encapsulated rather than aggregated is supported by energy dispersive X-ray (EDX) measurements showing Pt uniformly dispersed on the ZrO_2 surface (Figure S7), and by the appearance of Pt-(O)-Pt bonds in the Pt L_3-edge EXAFS of Pt/ZRO-5, Pt/ZRO-6, and Pt/ZRO-9 heat-treated at 500 °C (Figure S2(b)). When a-ZrO_2 was calcined, it underwent a transformation to the monoclinic phase, which improved the dispersion and catalytic activity of the supported Pt. Figure 5(a) presents the XRD patterns of ZRO-6 samples subjected to various thermal treatment at 500, 700, and 900 °C. The as-received ZRO-6 was initially amorphous, but upon calcination, it underwent a progressive crystallization into the m-ZrO_2 phase, as evidenced by the emergence and intensification of characteristic diffraction peaks. The transformation became more pronounced with increasing calcination temperature, confirming a temperature-dependent phase evolution from amorphous to crystalline. Figure S8 shows the BET specific surface areas of Pt/ZRO-6 catalysts prepared from these thermally treated supports. A distinct inverse relationship was observed between calcination temperature and surface area: as the heat-treatment temperature increased, the specific surface area systematically declined. This decrease is attributed to particle growth of ZrO_2 and densification associated with crystallization at elevated temperatures. Hydrosilylation of ethynylbenzene over catalysts prepared using ZRO-6 annealed at 500, 700, and 900 °C, resulting in progressive crystallization into the monoclinic phase, revealed a positive correlation between support annealing temperature and product yield (Figure S9). This trend suggests that increased crystallinity of m-ZrO_2 enhances catalytic performance. EXAFS analysis of the catalyst prepared using ZRO-6 annealed at 900 °C exhibited a weak Pt–O bonding signal while appearance of the Pt-Pt peak in the radial distribution function (Figure 5(b)). The $k^3\chi(k)$ data corresponding to Figure 5(b) is shown in Figure S10. The low intensity of the Pt-O peak in Figure 5(b) implies limited Pt aggregation and hints at the possible formation of dispersed Pt nanoparticles. H_2-TPR measurements showed that the amount of hydrogen consumed decreased with increasing annealing temperature of ZRO-6 (Figure S11). This behavior suggests that higher crystallinity of m-ZrO_2 facilitates the stabilization of Pt^0, in agreement with the Pt L_3-edge EXAFS shown in Figure 5(b).

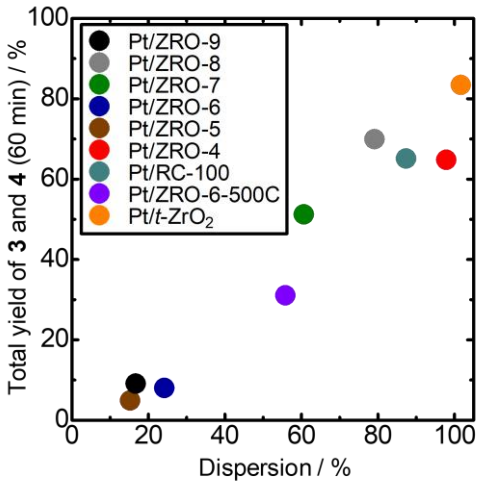

Figure 4. *Dependency of total yields of* **3** *and* **4** *on Pt dispersion.*

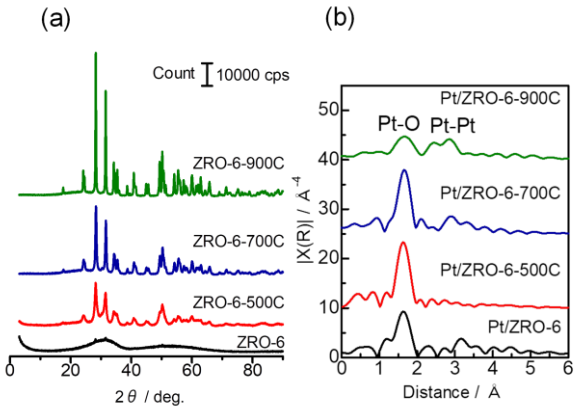

Figure 5. (a) *XRD patterns of ZRO-6 samples that were either untreated or heat-treated at 500 °C, 700 °C, and 900 °C. (b) Pt L_3-edge EXAFS radial distribution functions of Pt on ZRO-6 and those precalcined at 500, 700 and 900 °C. Fourier transform range was 3.0-14.7 Å^{-1}.*

Comparison of Pt dispersion and reusability of the Pt loaded on m-ZrO_2 and t-ZrO_2 supports

In order to compare the catalytic properties and structures of Pt catalysts supported on RC-100 (m-ZrO_2) and t-ZrO_2, we performed repeated reaction in the hydrosilylation. When the reaction was repeated 10 times for RC-100 and t-ZrO_2, a significant decrease in yield was observed in the Pt/t-ZrO_2 system from the third reaction while the improved recyclability was observed in Pt/RC-100 (Figure 6). The Pt L_3-edge EXAFS of both Pt/t-ZrO_2 and Pt/m-ZrO_2 after reaction revealed relatively dispersed form of Pt oxide was retained because only the Pt-O bond appeared in the EXAFS-FT (Figure S12(b)). Furthermore, the dispersion and structure of Pt/RC-100 and Pt/t-ZrO_2 were compared. When varying the Pt loading (1.0–2.0 wt%) for RC-100 and t-ZrO_2, higher Pt dispersion was observed in Pt/RC-100 compared with that of Pt/t-ZrO_2 (Figure 7(a)). Based on the EXAFS radial distribution function for each Pt loading, no Pt-Pt bonds were observed in

either RC-100 or t-ZrO_2 at 1.0 wt%, indicating atomic dispersion (Figure 7(b)). However, at Pt loadings of 1.5 wt% or higher, Pt-Pt bonds were observed in t-ZrO_2, confirming that Pt tends to aggregate at higher loadings in t-ZrO_2. In the Pt L_3-edge EXAFS of 2.0 wt% Pt/t-ZrO_2 shown in Figure 7(b), the peak assignable to metal Pt-Pt bonding was clearly observed, suggesting the presence of more aggregated metal Pt. In contrast, the Pt-Pt bond was hardly observed in the Pt L_3-edge EXAFS of 2.0 wt% Pt/m-ZrO_2, while Pt-O bonds were observed, meaning the strong interaction between oxidized Pt species with the surface of m-ZrO_2. In agreement with the fact, in the $k^3\chi(k)$ (Figure S13), the spectra of former (Pt/t-ZrO_2) exhibited a rapid oscillation originating from Pt-Pt bonding particularly in the samples with 2.0 wt% Pt, whereas those of the latter (Pt/m-ZrO_2) exhibited only a slow oscillation due to Pt-O bonding. These results indicate that there is no significant difference between m- and t-ZrO_2 in samples with a Pt loading of 1.0 wt%, but that the m-ZrO_2 is a more effective support for dispersing Pt in samples with a loading of 2.0 wt%. Based on these results, it is suggested that in Pt/ZrO_2 catalysts, when the ZrO_2 crystalline phase of the support is m-ZrO_2, it exhibits good reusability and does not cause a decrease in Pt dispersion even at high loading amounts. This indicates that m-ZrO_2 strongly binds Pt to the support surface, thereby suppressing the sintering during thermal treatment. The stronger bonding of Pt to t-ZrO_2 compared to m-ZrO_2 is also supported by analysis of the Pt L_3-edge XANES (Figure S14, 15). Specifically, by calculating the ratio of Pt^0 to Pt^{4+} from the weighted average of the pattern fitting (Figure S14) results for the Pt-L_3 edge XANES of the corresponding sample in Figure 7(b), using those of Pt foil and PtO_2, we found that 85-96% of Pt in Pt/m-ZrO_2 and approximately 44% of Pt in Pt/t-ZrO_2 were found to be Pt^{4+} (Figure S15). The difference indicated that Pt oxide existed stably in m-ZrO_2.

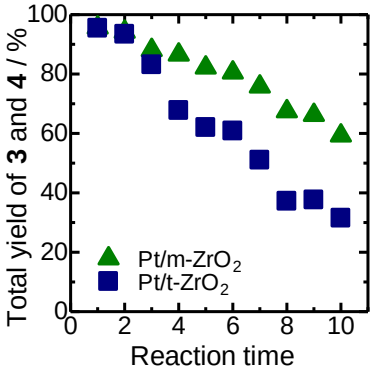

Figure 6. *Relationship between the number of reactions and the yield of the hydrosilylation reaction of Pt/ZrO_2 catalysts using RC-100 (m-ZrO_2) and t-ZrO_2. The reaction time of the horizontal axis indicated the initial reaction plus the number of times it was reused. The 0.7 wt% Pt/ZrO_2 catalyst after reaction was separated by centrifugation, dried overnight in a 70°C oven, and then used for subsequent reactions without pretreatment. This process was repeated before repeated reactions.*

Figure 8(a) and (b) show TEM images of samples in which 2 wt%-Pt was supported on RC-100 (m-ZrO_2) and t-ZrO_2, respectively, and then calcined at 500°C. In the TEM image of Pt/m-ZrO_2 image, finely dispersed Pt particles with a diameter of 1-2 nm were observed, whereas angular grains of 10-50 nm were observed in the image of Pt/t-ZrO_2. The fact was consistent with the dispersion and EXAFS data, which showed that the dispersion of Pt/m-ZrO_2 was higher than that of Pt/t-ZrO_2 (Figure 7(a)).

Conclusion

In this study, Pt was supported on three types of zirconia-amorphous, tetragonal, and monoclinic-to investigate the correlation between Pt dispersion and the zirconia crystal phase. The results suggest that in amorphous zirconia, Pt likely immersed into the ZrO_2 interior, causing the loss of active sites and resulting in low activity for hydrosilylation. In contrast, this phenomenon did not occur on tetragonal or monoclinic zirconia, leading to high activity of Pt. However, when comparing samples with Pt loading levels of 1.5 wt% or higher, the monoclinic zirconia support exhibited superior Pt dispersion and activity compared to the tetragonal zirconia support. This is likely due to the -OH groups originating from surface defects in the monoclinic zirconia promoting high Pt dispersion.

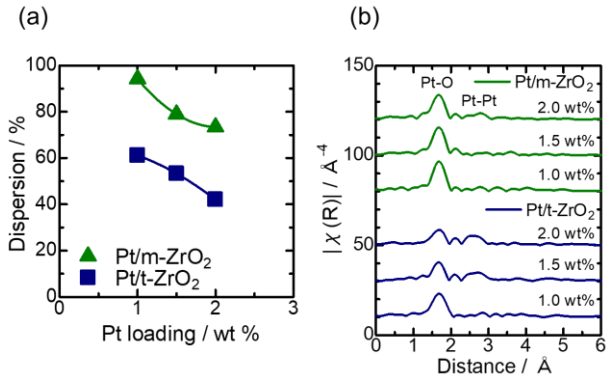

Figure 7. *Relationship between (a) Pt loading and Pt dispersion in Pt/RC-100 (m-ZrO_2) and Pt/t-ZrO_2. (b) Pt L_3-edge EXAFS radial distribution function of Pt/ZrO_2 for each Pt loading. Fourier transform range was 3.0-15.9 Å.*[1]

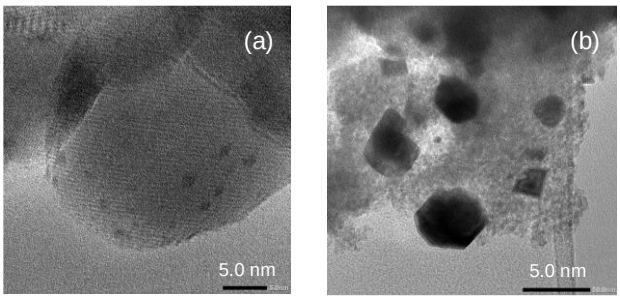

Figure 8. *TEM images of (a) Pt/RC-100 (m-ZrO_2) and (b) Pt/t-ZrO_2. The sample was prepared after impregnation of Pt(acac)$_2$ on the ZrO_2 supports, followed by calcination in air at 500 °C. Pt loading: 2.0 wt%.*

Experimental Section

Catalyst preparation: Pt-supported ZrO_2 (Pt/ZrO_2) catalysts were prepared via the impregnation method. 14.1 mg of bis(acetylacetonato)platinum(II) (hereafter referred to as Pt(acac)$_2$) was dissolved in 50 mL of acetone and mixed with 1.0 g of ZrO_2, resulting in a Pt loading of 0.7 wt%. Seven kinds of ZrO_2 supports (JRC-ZRO-4, JRC-ZRO-5, JRC-ZRO-6, JRC-ZRO-7, JRC-ZRO-8, JRC-ZRO-9 and RC-100) were supplied from Japan Reference Catalyst. Information on ZrO_2 supports is summarized in Table 1. Pt(acac)$_2$ was supplied by FUJIFILM Wako Pure Chemical Industries Ltd. The mixture was stirred and subsequently evaporated to dryness using a rotary evaporator at 30 °C. The resulting solid was ground in an agate mortar, transferred to a ceramic crucible, and calcined in air at 500 °C for 3 h (heating rate: 10 K min^{-1}), followed by spontaneous cooling to room temperature. The final catalysts were ground again and stored in airtight vials prior to use. The catalysts are denoted as Pt/Support; for instance, Pt/ZRO-4 indicates Pt supported on ZRO-4 and calcined at 500 °C. Amorphous ZRO-6 samples pre-calcined before Pt loading are denoted as Support-x °C, where x represents the pre-calcination temperature (e.g., ZRO-6-600C refers to JRC-ZRO-6 calcined at 600 °C prior to Pt impregnation and subsequent final calcination at 500 °C). As

a separate series from the above samples, Pt/ZrO_2 were also prepared by supporting 1.0 - 2.0 wt% Pt ($Pt(acac)_2$ was supplied by Tokyo Chemical Industry Co.) on ZrO_2 pre-calcined at 700 °C. Tetragonal-phase ZrO_2 (t-ZrO_2) was synthesized using the sol-gel method.[24] First, 12.0266 g of zirconyl nitrate hydrate ($ZrO(NO_3)_2{\cdot}2H_2O$, FUJIFILM Wako Pure Chemical Industries, Ltd.) was dissolved in 1000 mL of deionized water under stirring (300 rpm). Ethylenediamine was added dropwise until the pH reached 11. The resulting solution was refluxed at 100 °C for 48 h with continuous stirring (Chemist Plaza CP-400, SIBATA Chemical Co.). The resulting precipitate was recovered by centrifugation, thoroughly washed with deionized water, and dried at 110 °C overnight. The dried solid was ground and calcined in a muffle furnace at 700 °C for 3 h (heating rate: 10 K min^{-1}), then ground again for further use.

Catalyst characterization: The specific surface area of the catalysts was measured by nitrogen adsorption using the BET multipoint method. Approximately 0.1 g sample was degassed by vacuum heating at 300 °C prior to analysis on a BELSORP-mini-X system (Microtrac BEL). X-ray diffraction (XRD) was employed to determine the crystalline phases using a MiniFlex diffractometer (Rigaku) with Cu-*Kα* radiation (λ = 1.5406 Å), scanned over a 2θ range of 5 - 90° at 10° min^{-1}. Hydrogen temperature-programmed reduction (H_2-TPR) was conducted on 0.1 - 0.2 g of catalyst using a BELCAT II instrument (MicrotracBEL Co.) to investigate the reduction properties of the prepared catalysts. Samples were pretreated under N_2 flow, then heated to 650 °C at 10 K min^{-1} under a H_2/Ar flow. Pt dispersion was quantified via CO pulse chemisorption assuming a 1:1 Pt/CO stoichiometry under controlled conditions. X-ray absorption fine structure (XAFS) spectroscopy was performed to examine the local electronic and coordination structure of Pt in the catalysts. The

Table 1. List of ZrO_2 used for support of Pt.

ZrO_2 Support	Sample Name	Source
ZRO-4	JRC-ZRO-4	Reference Catalyst, Catalysis Society of Japan
ZRO-5	JRC-ZRO-5	Reference Catalyst, Catalysis Society of Japan
ZRO-6	JRC-ZRO-6	Reference Catalyst, Catalysis Society of Japan
ZRO-7	JRC-ZRO-7	Reference Catalyst, Catalysis Society of Japan
ZRO-8	JRC-ZRO-8	Reference Catalyst, Catalysis Society of Japan
ZRO-9	JRC-ZRO-9	Reference Catalyst, Catalysis Society of Japan
RC-100	RC-100	Daiichi Kigenso Kagaku Kogyo Co.
t-ZrO_2	t-ZrO_2	Prepared according to the literature[24]

experiments were performed at the High Energy Accelerator Research Organization Photon Factory (KEK-PF BL-9C, BL-12C) using a Si(111) monochromator (Proposal No.: 2024G563). Data acquisition was carried out via the fluorescence method using a 7-element silicon drift defector except for reference samples. XAFS data of the reference samples were collected with a transmission mode using two ion chambers (I_0: Ar15% + N_2 85%, I: Ar 100%). For each measurement for XAFS of Pt/ZrO_2, 0.1 g of catalyst was compressed into a 7 mm-diameter pellet. Data processing and analysis were conducted using REX2000 (Rigaku). A JEM-2100 microscope (JEOL Co.) equipped with an was used to take TEM images of the Pt/ZrO_2 samples, which was operated at 200 kV. For the preparation of the specimen, a suspension of the Pt/ZrO_2 sample in ethanol was dropped onto Cu grids with a C-coated porous thin membrane. XPS data were collected on a JEOL JPS-9030 spectrometer with a Mg Kα emission line (hν = 1253.6 eV). Sample charge compensation was controlled by referencing the O 1 s line at 532 eV.

Hydrosilylation reaction: The hydrosilylation reaction was performed in a batch reactor under ambient air to produce dimethylphenyl-1-phenylethylsilane (**3**) and dimethylphenyl[(E)-styryl]silane (**4**) as disubstituted alkenes. A Chemist Plaza CP-1000 reactor (SIBATA Chemical) was employed for the experiments. The reaction mixture consisted of catalyst (62 mg), ethynylbenzene (**2**, 1.1 mmol, Tokyo Chemical Industry Co. Ltd.), dimethylphenylsilane (**1**, 1.0 mmol, Tokyo Chemical Industry Co. Ltd.), tridecane (1.0 mmol, Fujifilm Wako Pure Chemical Industries Ltd.) as an internal standard, and 5 mL of toluene (Fujifilm Wako Pure Chemical Industries Ltd.) as solvent. The reaction mixture was stirred at 600 rpm and heated to 87 °C for 5 h. Upon completion, the mixture was cooled to room temperature and the supernatant was collected using a Pasteur pipette. It was then diluted fourfold with acetone and centrifuged to remove residual solids. Product composition was determined by GC with a flame ionization detector (GC-FID) using a SHIMADZU GC-2025 system equipped with an InertCap1 column (GL Science Co.). For the recycle use of Pt/ZrO_2, first the reaction was performed at 100 °C for 5 h. The catalyst was separated by centrifugation, dried overnight in an oven at 70 °C, and then reused in the subsequent reactions. The ^1H (400 MHz) and ^{13}C (100 MHz) NMR spectra were recorded in $CDCl_3$ using a JEOL ECZ-500 spectrometer (JEOL).

Supporting Information

Detailed Characterization and catalytic performance data of Pt/ZrO_2 are given in the Supporting Information at https://insuf.org/icms/icms.2025.02171SI.pdf

Author Information

Corresponding Author
Kazu Okumura - Department of Applied Chemistry, School of Advanced Engineering, Kogakuin University, 2665-1 Nakano-machi Hachioji-city, 192-0015, Tokyo, Japan.
Email: okmr@cc.kogakuin.ac.jp
https://orcid.org/0000-0002-7952-3482

Authors
Yuki Aoki - Department of Applied Chemistry, School of Advanced Engineering, Kogakuin University, 2665-1 Nakano-machi Hachioji-city, 192-0015, Tokyo, Japan.
Anas Abdullahi - Department of Applied Chemistry, School of Advanced Engineering, Kogakuin University, 2665-1 Nakano-machi Hachioji-city, 192-0015, Tokyo, Japan.
https://orcid.org/0009-0003-2409-809X
Mustapha G. Mohammed- Department of Chemical Engineering, Faculty of Engineering, Universiti Malaya, 50603, Kuala Lumpur, Malaysia.
Kotaro Kawaguchi - Department of Applied Chemistry, School of Advanced Engineering, Kogakuin University, 2665-1 Nakano-machi Hachioji-city, 192-0015, Tokyo, Japan.

Author Contribution Declaration

Declare the author contribution in brief here. e.g., Yuki Aoki, Kotaro Kawaguchi, and Kazu Okumura designs the article, conceived the review/research plan and experimental strategy. Anas Abdullahi confirmed the manuscript preparation and assist in daily laboratory supervision, wrote manuscript. Mustapha G. Mohammed prepared draft manuscript.

Funding Sources

Ministry of Education, Science, Sports and Culture, Grant-in-Aid for Scientific Research (C), 22K04833, 2022-2024 and 25K08389, 2025-2027 for financial support.

Data Availability Declaration

The authors declare that the data supporting the findings are available within the article and its Supplementary Information file.

Declaration of competing interest

The author declares no known competing financial interests.

Acknowledgements

This research was supported by the Ministry of Education, Science, Sports and Culture, Grant-in-Aid for Scientific Research (C), 22K04833, 2022-2024 and 25K08389, 2025-2027.

References

1. B. Marciniec. Hydrosilylation and Related Reactions of Silicon Compounds. *in Applied Homogeneous Catalysis with Organometallic Compounds*, **2002**, pp. 491-512, https://doi.org/10.1002/9783527651733.ch8
2. B. Marciniec. Catalysis by transition metal complexes of alkene silylation–recent progress and mechanistic implications. *Coord. Chem. Rev.*, **2005**, *249*, 2374. https://doi.org/10.1016/j.ccr.2005.02.025
3. R. Murugavel, A. Voigt, M. G. Walawalkar, H. W. Roesky. Hetero- and Metallasiloxanes Derived from Silanediols, Disilanols, Silanetriols, and Trisilanols. *Chem. Rev.*, **1996**, *96*, 2205. https://doi.org/10.1021/cr9500747
4. Y. K. Mirza, P. S. Bera, S. B. Mohite, A. K. Pandey, M. Bera. Silanes as a versatile hydride source for Ni–H catalysis: a promising tool for π-hydro functionalization. *Org. Chem. Front.*, **2024**, *11* 4290, https://doi.org/10.1039/D4QO00860J
5. Y. Nakajima, S. Shimada. Hydrosilylation reaction of olefins: recent advances and perspectives. *RSC Adv.*, **2015**, *5*, 20603. https://doi.org/10.1039/C4RA17281G
6. G. Pan, C. Hu, S. Hong, H. Li, D. Yu, C. Cui, Q. Li, N. Liang, Y. Jiang, L. Zheng, L. Jiang, Y. Liu. Biomimetic caged platinum catalyst for hydrosilylation reaction with high site selectivity. *Nat. Commun.*, **2021**, 12, 64. https://doi.org/10.1038/s41467-020-20233-w
7. Y. Gong, Q. Mou, D. Peng, F. Wang, J. Qin, J. Qin, Y. Ding. New insight into the mechanism of Pt(0)-catalyzed hydrosilylation reaction of (CH(3))(3)SiH with CH(2)CHSi(CH(3))(3). (*in eng*), *J Mol Graph Model*, **2022**, *117*, 108294. https://doi.org/10.1016/j.jmgm.2022.108294
8. I. E. Markó, S. Stérin, O. Buisine, G. Mignani, P. Branlard, B. Tinant, J. P. Declercq. Selective and Efficient Platinum(0)-Carbene Complexes As Hydrosilylation Catalysts. *Science*, **2002**, *298*, 204. https://doi.org/10.1126/science.1073338
9. B. P. Maliszewski, N. V. Tzouras, S. G. Guillet, M. Saab, M. Beliš, K. V. Hecke, F. Nahra, S. P. Nolan. A general protocol for the synthesis of Pt-NHC (NHC = N-heterocyclic carbene) hydrosilylation catalysts. *Dalton Trans.,* **2020**, *49*, 14673. https://doi.org/10.1039/D0DT03480K
10. O. Buisine, G. B. Gelloz, J. F. Brière, S. Stérin, G. Mignani, P. Branlard, B. Tinant, J. P. Declercq, I. E. Markó. Second generation N-heterocyclic carbene–Pt(0) complexes as efficient catalysts for the hydrosilylation of alkenes. *Chem. Commun.*, **2005**, *30*, 3856, https://doi.org/10.1039/B506369H
11. J. C. Bernhammer, H. V. Huynh. Platinum(II) Complexes with Thioether-Functionalized Benzimidazolin-2-ylidene Ligands: Synthesis, Structural Characterization, and Application in Hydroelementation Reactions. *Organometallics*, **2014**, *33*, 172. https://doi.org/10.1021/om400929t
12. A. J. Holwell. Global Release Liner Industry Conference 2008. *Platinum Metals Review*, **2008**, *52*, 243. https://doi.org/10.1595/147106708X366975
13. H. Yang, Z. Zhou, C. Tang, F. Chen. Recent advances in heterogeneous hydrosilylation of unsaturated carbon-carbon bonds. *Chi. Chem. Lett.*, **2024**, *35*, 109257. https://doi.org/10.1016/j.cclet.2023.109257
14. L. Zhang, M. Zhou, A. Wang, T. Zhang. Selective Hydrogenation over Supported Metal Catalysts: From Nanoparticles to Single Atoms. *Chem. Rev.*, **2020**, *120*, 683. https://doi.org/10.1021/acs.chemrev.9b00230
15. X. Cui, K. Junge, X. Dai, C. Kreyenschulte, M. M. Pohl, S. Wohlrab, F. Shi, A. Brückner, M. Beller. Synthesis of Single Atom Based Heterogeneous Platinum Catalysts: High Selectivity and Activity for Hydrosilylation Reactions. *ACS Cent. Sci.*, **2017**, *3*, 580. https://doi.org/10.1021/acscentsci.7b00105
16. Y. Chen, S. Ji, W. Sun, W. Chen, J. Dong, J. Wen, J. Zhang, Z. Li, L. Zheng, C. Chen, Q. Peng, D. Wang, Y. Li. Discovering Partially Charged Single-Atom Pt for Enhanced Anti-Markovnikov Alkene Hydrosilylation. *J. Am. Chem. Soc.*, **2018**, *140*, 7407. https://doi.org/10.1021/jacs.8b03121
17. C. J. Kong, S. E. Gilliland, B. R. Clark, B. F. Gupton. Highly-active, graphene-supported platinum catalyst for the solventless hydrosilylation of olefins. *Chem. Commun.*, **2018**, *54*, 13343. https://doi.org/10.1039/c8cc07641c
18. K. Okumura, R. Chihara, A. Abdullahi, M. Kato. Characterization of the active species in the aerobic oxidation of benzyl alcohol catalyzed by Ru/ZrO_2. *Mol. Catal.*, **2025**, *573*, 114820. https://doi.org/10.1016/j.mcat.2025.114820
19. T. Zhang, M. Li, P. Zheng, J. Li, J. Gao, H. He, F. Gu, W. Chen, Y. Ji, Z. Zhong, D. Bai, G. Xu, F. Su. Highly Efficient Hydrosilylation of Ethyne over Pt/ZrO_2 Catalysts with Size-Dependent Metal–Support Interactions. *Ind. Eng. Chem. Res.*, **2022**, *61*, 18703. https://doi.org/10.1021/acs.iecr.2c03553
20. M. Li, S. Zhao, J. Li, X. Chen, Y. Ji, H. Yu, D. Bai, G. Xu, Z. Zhong, F. Su. Partially charged single-atom Ru supported on ZrO_2 nanocrystals for highly efficient ethylene hydrosilylation with triethoxysilane. Nano Res., **2022**, *15*, 5857. https://doi.org/10.1007/s12274-022-4227-4
21. K. Okumura, S. Aikawa, Y. Aoki, A. Abdullahi, M. G. Mohammed. Rational Design of Pt Supported Catalysts for Hydrosilylation: Influence of Support and Calcination Temperature: Heterogeneous Catalysis. *Innov. Chem. Mater. Sustain.*, **2025**, 2, 74. http://doi.org/10.63654/icms.2025.02074
22. K. Okumura, S. Sugihara, Y. Yasui, R. Sugiyama, A. Ahmed, A. Abdullahi. Solvent-Free Synthesis and Applications of Highly Dispersed Ruthenium Catalysts Prepared by Solid-Phase Mixing. *ACS Omega*, **2025**, *10*, 29510. https://doi.org/10.1021/acsomega.5c02830
23. E. Ramírez-Oliva, A. Hernández, J. M. Martínez-Rosales, A. Aguilar-Elguezabal, G. Herrera-Pérez, J. Cervantes. Effect of the synthetic method of Pt/MgO in the hydrosilylation of phenylacetylene. *Arkivoc*, **2006**, 126.
24. V. G. Deshmane, Y. G. Adewuyi. Synthesis of thermally stable, high surface area, nanocrystalline mesoporous tetragonal zirconium dioxide (ZrO2): Effects of different process parameters. *Micropor. Mesopor. Mater.*, **2012**, 148, 88. https://doi.org/10.1016/j.micromeso.2011.07.012